Sensors and Actuators A 220 (2014) 69–75

Contents lists available at ScienceDirect

Sensors and Actuators A: Physical

journal homepage: www.elsevier.com/locate/sna

An auto-parametrically excited vibration energy harvester

Yu Jia*, Ashwin A. Seshia

Department of Engineering, University of Cambridge, Cambridge CB2 1PZ, UK

ARTICLE INFO

Article history:
Received 18 April 2014
Received in revised form
11 September 2014
Accepted 12 September 2014
Available online 22 September 2014

Keywords:
Auto-parametric
Resonance
Initiation threshold
Piezoelectric
Vibration energy harvesting

ABSTRACT

Parametric resonance, as a resonant amplification phenomenon, is a superior mechanical amplifier than direct resonance and has already been demonstrated to possess the potential to offer over an order of magnitude higher power output for vibration energy harvesting than the conventional direct excitation. However, unlike directly excited systems, parametric resonance has a minimum threshold amplitude that must be attained prior to its activation. The authors have previously presented the addition of initial spring designs to minimise this threshold, through non-resonant direct amplification of the base excitation that is subsequently fed into the parametric resonator. This paper explores the integration of auto-parametric resonance, as a form of resonant amplification of the base excitation, to further minimise this activation criterion and realise the profitable regions of parametric resonance at even lower input acceleration levels. Numerical and experimental results have demonstrated in excess of an order of magnitude reduction in the initiation threshold amplitude for an auto-parametric resonator (~0.6 ms^{-2}) as well as several folds lower for a parametric resonator with a non-resonant base amplifier (~4.0 ms^{-2}), as oppose to a sole parametric resonator without any threshold reduction mechanisms (10's ms^{-2}). Therefore, the superior power performance of parametric resonance over direct resonance has been activated and demonstrated at much lower input levels.

1. Introduction

Vibration energy harvesting (VEH) has gained immense popularity in recent years. However, the absolute attainable power level remains an issue in practical applications. Resonant-based vibration energy harvesters have been the core of the technology to amplify the base excitation in order to maximise the total amount of mechanical energy that can be captured [1,2]. Attempts to improve the power output, based on design and mechanical mechanisms, include: system parameter optimisation [3], array addition around the same frequency range [4], bending of resonant peaks due to Duffing nonlinearities [5,6], jumping of potential wells for bi-stabile [7,8] or multi-stable systems [9], stochastic resonance [10], coupling of multiple transducers such as piezoelectric and electromagnetic transducers [11] as well as frequency up conversion of either linear [12,13] or rotational generators [14,15]. Yet, most of these either yielded no noticeable improvement or relatively modest enhancement (within a few folds) in terms of the power density for a given acceleration.

Overwhelming majority of the conventional approaches, either linear or nonlinear, have primarily relied upon directly excited resonance. The authors however, have previously demonstrated an alternative: parametric resonance at both macro-scale [16,17] and MEMS scale [18,19], outperforming the same device driven into direct resonance by over an order of magnitude in power output when subjected to the same acceleration level. Instead of forcing a direct response from a system associated with direct resonance, parametric resonance relies on the periodic modulation in one of the system parameters to internally accumulate energy. Despite the promising potential of parametric resonance over its direct counterpart, the drive acceleration must attain a damping-dependant initiation threshold amplitude prior to activating it altogether [20,21].

Previous parametric resonant harvesters developed by the authors [17,18] have included an additional initial spring structure, which serves to amplify the base excitation, coupling into the parametric resonator. However, prior to this paper, the authors have only reported non-resonant amplification of the base excitation by the initial spring. Nonetheless, this design approach has already experimentally demonstrated the ability to reduce the initiation threshold amplitude of a typical sole parametric resonant VEH prototype from 10's ms^{-2} to 1's ms^{-2}. This allows access to the profitable regions of parametric resonance at lower and more practical input acceleration levels.

This paper builds on the previous work and proposes the employment of auto-parametric resonance, as a means of resonant

* Corresponding author. Tel.: +44 7748839904.
E-mail addresses: yj252@cam.ac.uk (Y. Jia), aas41@cam.ac.uk (A.A. Seshia).

http://dx.doi.org/10.1016/j.sna.2014.09.012

amplification of the base excitation, to further reduce the initiation threshold amplitude of the parametric resonant harvester device in an attempt to render this threshold limitation practically negligible (targeting 0.1's ms^{-2}). Contrary to the external excitation induced hetero-parametric resonance, auto-parametric resonance is triggered by aligning the longitudinal and transverse natural frequencies within the system in a 2:1 ratio. The classical example is a pendulum suspended off an elastic spring where the natural frequency of the spring is twice that of the pendulum [22].

The various configurations of resonant systems explored in this paper are delineated as the following.

- *Direct resonator:* a resonating system that responds to direct excitation
- *(Plain) parametric resonator:* a resonating system that responds to parametric excitation, but has no additional mechanical mechanisms to minimise the initiation threshold amplitude
- *Parametric resonator with non-resonant base excitation amplification:* a parametric resonating system with an initial spring. The natural frequency of the initial spring is not twice that of the parametric resonator.
- *Auto-parametric resonator:* a parametric resonating system with an initial spring. The natural frequency of the initial spring is twice that of the parametric resonator.

2. Design and modelling

2.1. Design and analytical model

The design employed is shown in Fig. 1a, resembling an inverted T-shape. The primary parametric resonator is the vertically upright cantilever beam resting on a horizontal clamped-clamped initial spring. When a vertical driving force is applied, the initial spring is directly excited while the cantilever can be parametrically excited under the right conditions. For a configuration where the natural frequency of the initial spring ω_1 is twice the natural frequency of the cantilever ω_2, auto-parametric resonance, and therefore direct resonant amplification of the base excitation to feed into the parametric resonator, can be achieved. On the other hand, for configurations where $\omega_1 \neq 2\omega_2$, only non-resonant amplification of the base excitation can be achieved to drive the principal parametric resonance, as reported in previous studies [17,18].

Fig. 1b represents the mass-spring-damper equivalent of the system. Here, c_s, k_s, c_p, k_p, m_p, y and x denote damping of the initial spring, stiffness of the initial spring, damping of the parametric resonator, stiffness of the parametric resonator, effective mass of the system, displacement of the initial spring and displacement of the parametric resonator respectively.

The initial spring is able to transmit energy absorbed from the mechanical excitation to the subsidiary cantilever spring. However, x must possess an initial displacement to allow orthogonal propagation of vibration into the parametric resonator. This criterion can be bypassed by a vertically upright end mass configuration, drawing parallels from an inverted pendulum, to place the zero-displacement rest position in an unstable equilibrium. This study employs a clamped–clamped beam design as the initial spring for a cantilever-based parametric resonator. However, other spring designs, such as cantilever beams or membranes, for both the initial spring and the parametric resonator, are all theoretically possible.

The natural frequency of a typical firmly clamped cantilever beam is given by Eq. (1) [23].

$$\omega_0^2 = \frac{3EI}{(0.24m_b + m_l)l^3} \tag{1}$$

where, ω_0 is the natural frequency, E is the elastic modulus, I is the area moment of inertia, m_b is the beam mass, m_l is the proof mass and l is the beam length. The effective natural frequency of the cantilever in this T-shaped system will be a fraction of this relationship depending on the spring stiffness of the initial spring.

The natural frequency of a typical clamped-clamped beam with centred mass is given by Eq. (2) [23] and of an asymmetrically placed mass is given by Eq. (3).

$$\omega_0^2 = \frac{48EI}{\left(\frac{48m_b}{\pi^4} + m_l\right) l^3} \tag{2}$$

$$\omega_0^2 = \frac{9\sqrt{3}lEI}{ml_b(l^2 - l_b^2)^{3/2}} \tag{3}$$

where, l_a and l_b are two segments of the doubly clamped beam separated by the proof mass, $l_a + l_b = l$ and the effective mass m is placed at distance l_a from the origin measured from the clamped side of l_a. The x displacement of the subsidiary cantilever beam shifts the centre of mass for the clamped–clamped beam and affects its natural frequency accordingly, as given in Eq. (4). Though, this natural frequency variation is minimal and can be neglected in most simplified cases.

$$\omega_0^2 = \frac{9\sqrt{3}lEI}{m(l_b - x(t))\left(l^2 - (l_b - x(t))^2\right)^{3/2}} \tag{4}$$

The equations of motion for such a two degrees-of-freedom auto-parametric system with the direct-to-parametric

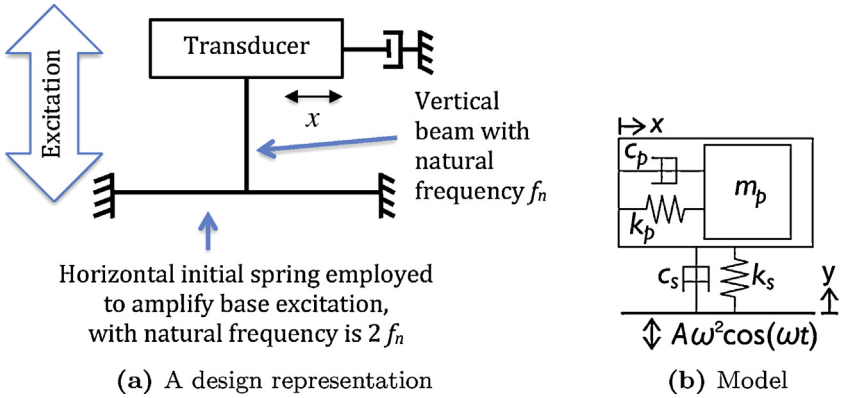

Fig. 1. Vertical cantilever parametric resonator with added horizontal initial spring to amplify the base excitation in order minimise the initiation threshold amplitude to access parametric resonance. For a direct resonator, the excitation is parallel to the displacement. Whereas, the excitation and displacement of parametric resonators are typically orthogonal to each other. A plain parametric resonator has no initial spring (c_s and k_s). For an auto-parametric resonator, the natural frequencies of the initial spring and the cantilever have a ratio of 2:1. A parametric resonator with non-resonant base excitation amplification does not have a 2:1 internal frequency ratio.

Table 1
Parameter values used for MATLAB simulation of the T-shaped system.

ζ_1	0.0125	ζ_2	0.005
ξ	3.5	μ	1

(initial-spring-to-cantilever) configuration can be represented by Eqs. (5) and (6) [24].

$$\ddot{y} + 2\zeta_1\omega_1\dot{y} + \omega_1^2 y - \xi\mu(\dot{x}^2 + x\ddot{x}) = \omega^2 A\cos\omega t \quad (5)$$

$$\ddot{x} + 2\zeta_2\omega_2\dot{x} + \omega_2^2 x - \xi\ddot{y}x = 0 \quad (6)$$

where, ω_1 and ω_2 are the natural frequencies of the doubly clamped initial spring and the subsidiary cantilever resonator respectively, ξ is the mode coupling coefficient, μ is the nonlinearity coefficient, ω is the drive frequency and A is the excitation displacement amplitude. The $\ddot{y}$ coefficient in equation 6 serves as the time function to induce the parameter modulation.

2.2. Numerical model

A numerical model of the presented T-shaped resonator, using the system parameter values shown in Table 1 (fitted to the experimental results presented in the next section), was constructed in MATLAB with ODE45 solver. Fig. 2 presents an example of the numerically simulated time domain response of both the direct resonant build-up of the initial spring and the parametric resonant build-up of the cantilever beam. For a scenario where $\omega = \omega_1 = 2\omega_2$, auto-parametric resonance can be activated.

Direct resonant oscillatory amplitude build up of the initial spring, as shown in Fig. 2a, is faster than that of the parametric resonance of the initial spring presented in Fig. 2b. However, when the parametric resonance of the cantilever does onset, the energy accumulated in the initial spring from direct resonant build up is internally transferred to the subsidiary cantilever in a parametric fashion.

As the oscillation of the parametric resonator starts to dominate and the system operates deeper within the Mathieu instability region, the mechanical energy stored in the system no longer returns to the direct resonator and the oscillatory amplitude of the direct resonator irreversibly diminishes [25] as can be seen with the 'pinch' in Fig. 2a after about 60 s. This 'pinch' is synchronised with the onset of parametric resonance in Fig. 2b.

While the response frequency of direct resonators always matches the excitation frequency, that of the parametric resonator lingers around the vicinity of the natural frequency regardless of the excitation frequency. Therefore, the first order parametric resonant response frequency of the cantilever (Fig. 2d) is half of both the excitation frequency and the response frequency of the direct resonator (Fig. 2c).

Fig. 3 presents the numerically simulated result of input acceleration versus response acceleration for the initial spring (dubbed 'Direct') and the cantilever parametric resonator (dubbed

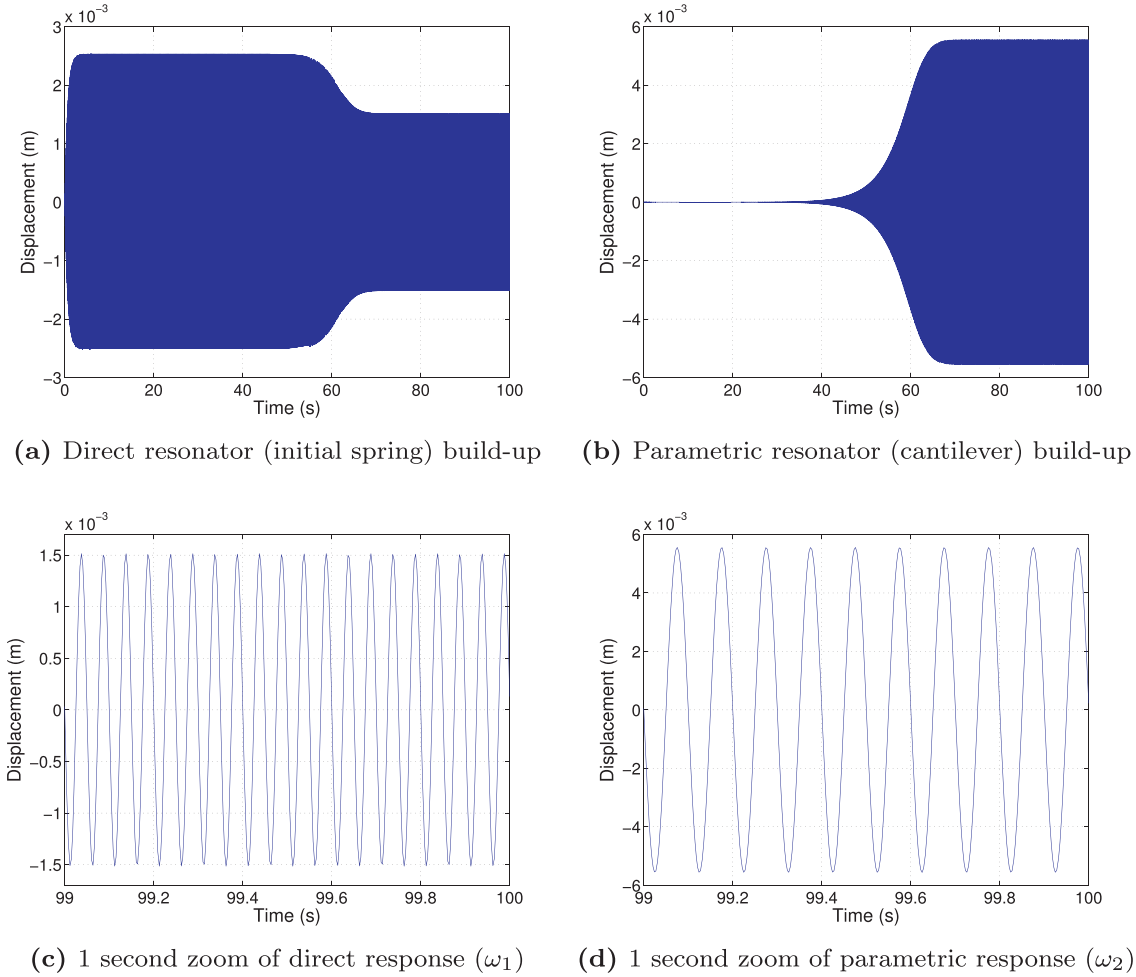

(a) Direct resonator (initial spring) build-up **(b)** Parametric resonator (cantilever) build-up

(c) 1 second zoom of direct response (ω_1) **(d)** 1 second zoom of parametric response (ω_2)

Fig. 2. Numerical simulation of auto-parametric resonant build for both the directly excited initial spring and the parametrically resonating cantilever when subjected to acceleration of 1 ms^{-2} and frequency $\omega = \omega_1 = 2\omega_2$, where ω_1 is the natural frequency of the initial spring and ω_2 is that of the parametric resonator. The oscillatory amplitude of the direct resonator diminishes (shown by the 'pinch') when parametric resonance onsets, as energy is irreversibly pumped into the parametric resonator.

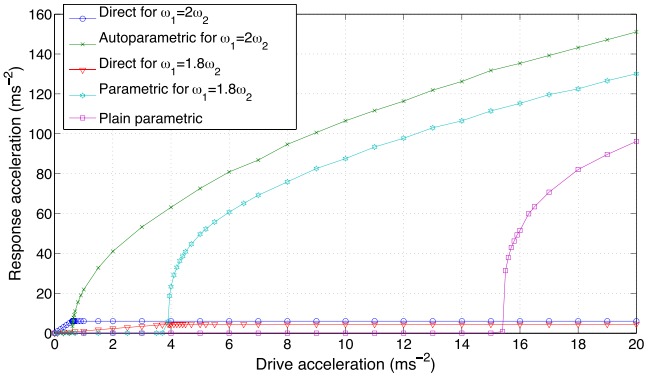

Fig. 3. Numerical input versus output acceleration for the two degrees-of-freedom direct resonator initial-spring (with natural frequency ω_1) and the parametric resonator cantilever (with natural frequency ω_2) system when: drive frequency $\omega = 2\omega_2 = \omega_1$ (auto-parametric) and $\omega = 2\omega_2 = 1.11\omega_1$ (parametric with non-resonant base excitation amplification). A plain parametric resonator without an initial spring structure was also simulated. The initiation threshold amplitude of parametric resonance for the auto-parametric case ($\omega_1 = 2\omega_2$) is 0.61 ms^{-2}, for the mismatched scenario ($\omega_1 = 1.8\omega_2$) is 3.9 ms^{-2} and for the plain parametric resonator is 15.4 ms^{-2}.

'Parametric'). Two scenarios are compared here: ω_1 is matched to $2\omega_2$ to activate auto-parametric resonance that involves resonant amplification of the base excitation by the initial spring; as well as mismatched frequencies ($\omega_1 = 1.8\omega_2$) to active parametric resonance with non-resonant amplification of the base excitation by the initial spring. Additionally, a comparable plain parametric resonator without the initial spring is also included here as a third scenario.

For the auto-parametric scenario ($\omega = 2\omega_2 = \omega_1$), the initial spring is driven into direct resonance, whereas the initial spring of the second scenario ($\omega = 2\omega_2 = 1.11\omega_1$) is driven off resonance by a factor of 1.11. Therefore, a weaker amplification of the base excitation is fed into the parametric resonator for the later case.

It can be seen from Fig. 3 that the auto-parametric case observed the onset of parametric resonance at a significantly lower acceleration level (0.61 ms^{-2}) than the non-resonant initial spring case (3.9 ms^{-2}); however, the response of both systems eventually converge at higher acceleration levels. The threshold summary of various numerically simulated configurations are listed below:

- Plain parametric resonator with no base excitation amplification: 15.4 ms^{-2}
- Parametric resonator with non-resonant base excitation amplification: 3.9 ms^{-2}
- Auto-parametric resonator (resonant base excitation amplification): 0.61 ms^{-2}

It can also be noted that upon activation of parametric resonance, the steady state solution of direct response of the initial spring no longer increase as any excess energy is irreversibly transferred to the subsidiary parametric resonator. This occurred at a lower drive acceleration level for the auto-parametric scenario, so the direct response of its initial spring was constrained earlier than its counterpart scenario.

3. Experimental apparatus

3.1. Device

Piezoceramic strips of dimensions 40 mm by 20 mm from APC International were employed as the mechanical-to-electrical transducer. These transducers were composed of bi-morph piezoelectric

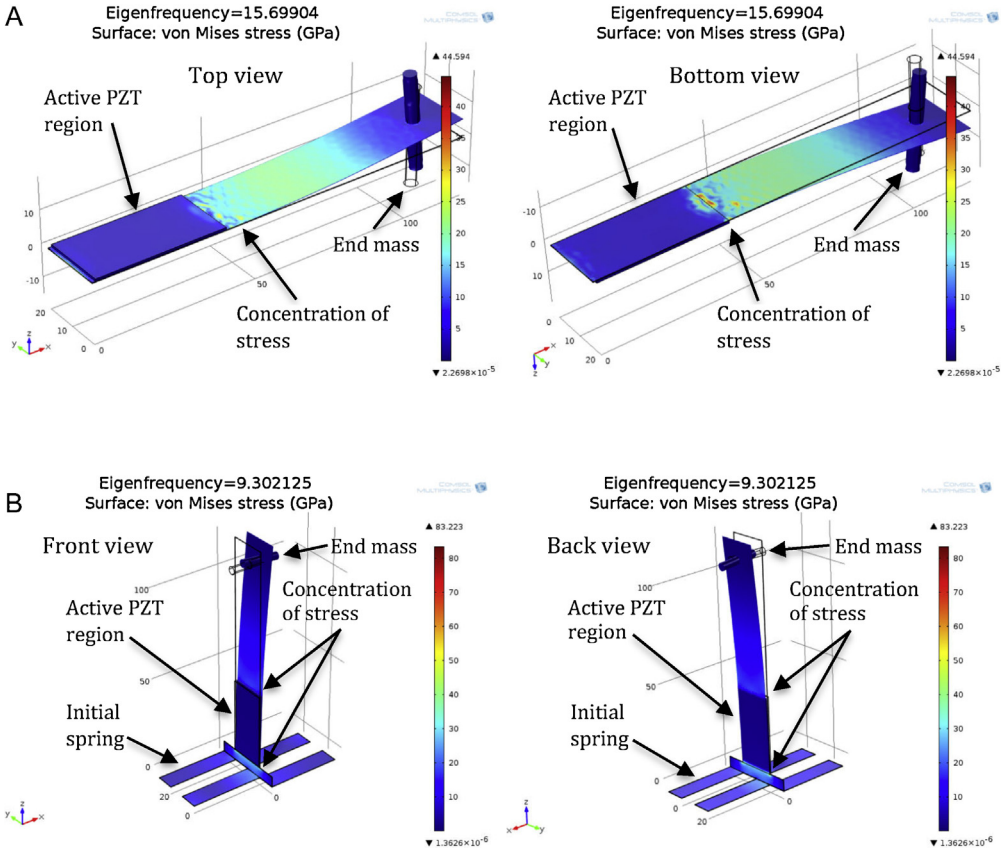

Fig. 4. COMSOL models of sole cantilever and initial-spring-cantilever resonators with piezoceramic strips attached towards the clamped end.

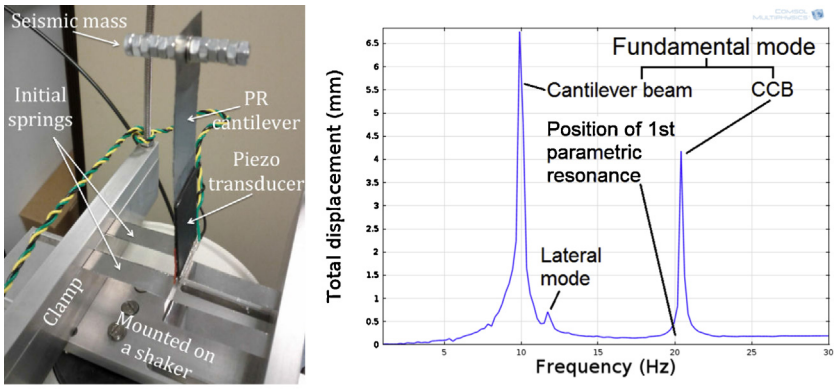

(a) Prototype (b) COMSOL frequency domain response

Fig. 5. T-shaped piezoelectric cantilever-based prototype with orthogonal initial spring structure. Both sides of the horizontal spring arms are on the same plane. Excitation is applied vertically. The upright cantilever beam acts primarily as a parametric resonator (PR), while the clamped–clamped beam (CCB) has a natural frequency approximately twice that of PR.

layers separated by a common ground electrode. The bi-morph is in turn sandwiched between poling electrodes with an electrically insulating varnish coating on the outer most structure. The total thickness is approximately 0.7 mm with capacitance in the order of 100's nF.

Cutoffs from mild steel shim of 101.6 μm thickness were employed as the spring of the resonator. Through attaching the piezoceramic onto the shim substrate using epoxy adhesive, two major design variants were constructed: a sole cantilever beam as well as a parametric resonator with orthogonal initial spring as shown in Fig. 4.

The mounted prototype device of the configuration with the initial spring is shown in Fig. 5a. COMSOL simulated frequency domain characteristics of this setup is shown in Fig. 5b. The fundamental direct resonant mode of the cantilever and the doubly clamped initial spring can be seen around the vicinity of 10 and 20 Hz, respectively. The first order parametric resonant mode of the cantilever would thus theoretically appear when the excitation frequency is around 20 Hz. This is not shown in the plot as COMSOL Multiphysics 4.2 currently lacks the physics describing the parametric resonant phenomenon.

Steel nuts are added on a screw near the free end of the cantilever to act as an adjustable seismic mass. Through adjustment of the value of the total mass, the positioning of the end mass along the cantilever beam as well as the positioning of the base clamps to vary the active length of the doubly-clamped initial spring, natural frequencies of both the initial spring and the cantilever can be tuned to either match or mismatch the 2:1 ratio.

Although it is relatively easy to construct and shape the steel shim, this prototype suffers from the significantly higher stiffness of the piezoceramic compared to the thin steel spring, which restricts the induced strain on the active transducer. In this particular implementation, the epoxy adhesive further increases the stiffness as a bonding layer and introduces additional damping between the spring and piezo layers. Despite the shortcomings of this apparatus, which compromises the absolute power output attainable, the piezoceramic still acts as a viable vibration sensor to achieve qualitative characterisation and a relative quantitative comparison when the prototype is driven into direct and parametric resonance.

4. Results and discussion

Fig. 6 illustrates an example of the transient response of the parametric resonator. The prolonged build-up characteristics of the parametric response is in qualitative agreement with the numerical simulation of Fig. 2. The time period of the parametric transient

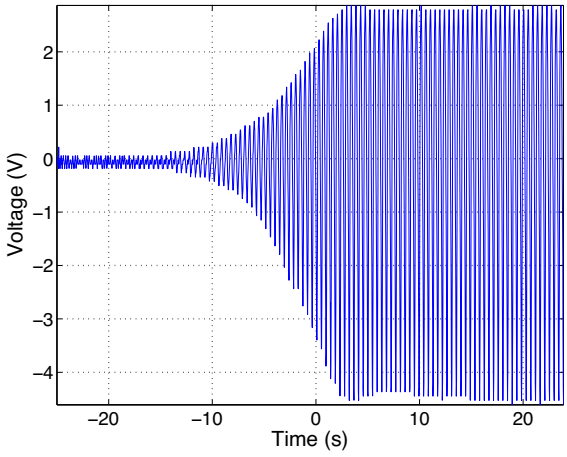

Fig. 6. Transient voltage response of the prototype when driven at 2 g of acceleration, showing the prolonged transient oscillatory build-up for parametric resonance.

build-up is dependent on the acceleration level and damping ratio. As the system operates deeper into the instability region, this transient build-up state becomes shorter and the amplitude is attainable more readily. The asymmetry in the peak to peak response is due to the mechanical asymmetry from the prototype.

The optimal parallel resistive load was experimentally matched to be in the order of 0.2–0.4 MΩ for the given frequency range. Fig. 7 presents the peak power response per excitation acceleration for a sole cantilever (SC) and a cantilever with initial spring structure (ISC). The amplification of base excitation by the initial spring in

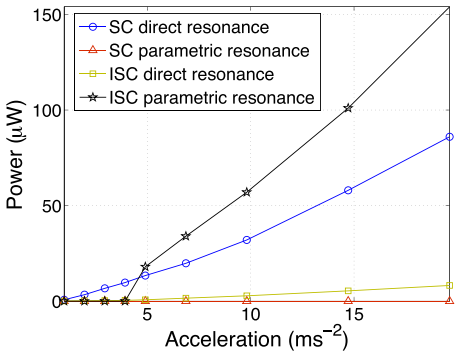

Fig. 7. Comparison between sole cantilever (SC) and cantilever with initial spring structure (ISC).

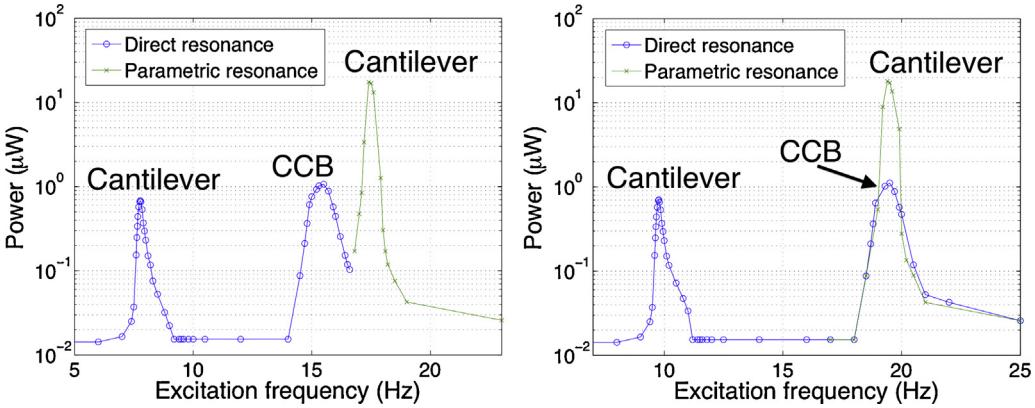

Fig. 8. Frequency tuned to exhibit parametric and auto-parametric resonance at ~ 5.0 ms^{-2}. CCB represents the clamped-clamped beam initial spring. The half power bandwidth for the cantilever direct resonant peak is ~ 0.25 Hz and that for the cantilever parametric resonant peak is ~ 0.55 Hz.

this scenario is non-resonant in nature. This plot serves to compare the two design configurations where the amplification of base excitation is either present or absent.

Within the scanned acceleration of up to 2 g, no onset of parametric resonance was observed for the sole cantilever. On the other hand, onset of parametric resonance for the cantilevers with initial springs initiated around 0.4 g. It can be seen that the initial-spring-cantilever (ISC) has lower mechanical efficiency than its sole cantilever (SC) counterpart. This is because in addition to the base excitation amplification effect of the initial spring, this additional degree-of-freedom also acts as a dashpot. For excitation in excess of 0.5 g of acceleration, the parametric resonant power response of ISC rapidly outperformed the direct resonant response of the SC, demonstrating the benefit and therefore the motivation to activate parametric resonance.

Fig. 8 presents the ISC prototype tuned to parametric resonance and auto-parametric resonance. The piezoelectric transducer was responsive to 1st transverse mode of the cantilever beam and the 1st transverse mode of the orthogonal clamped–clamped beam (CCB) initial spring. Through tuning the natural frequency of the CCB to match to twice the natural frequency of the cantilever, auto-parametric resonance was achieved.

A summary of experimentally measured initiation threshold amplitude of the various configurations are shown below,

- Plain parametric resonator with no base excitation amplification: >20 ms^{-2}
- Parametric resonator with non-resonant base excitation amplification: ~4.0 ms^{-2}
- Auto-parametric resonator (resonant base excitation amplification): ~0.6 ms^{-2}

The superior power performance advantage of parametric resonance is able to be activated at lower excitation amplitudes for the auto-parametric resonator. However, once the parametric resonance of the system with non-resonant base excitation amplification onsets, its steady state power amplitude quickly catches on with that of the auto-parametric resonator, as in agreement with the converging trend shown in the numerical result of Fig. 3.

As mentioned earlier and shown in the numerical result of Fig. 2d, a typical identifier of principal parametric resonance is where the response frequency is half of the excitation frequency. Within the auto-parametric vicinity shown in Fig. 8, an alternating modulation of energy transfer between the parametric resonant regime of the cantilever and linear harmonic resonant regime of the CCB was identified by the frequency signatures. These two fundamentally distinct regimes are not capable of simultaneous operational co-existence.

This is contrary to the irreversible parametric response observation made in the numerical model. A possible explanation could be due to the system operating at the borderline of the Mathieu stability loci and stochastic effects could push the system out of the instability zone. However, at higher excitation levels, the system operates deeper into the instability region (moving away from the loci) and auto-parametric resonance becomes irreversibly dominant over direct resonance of the CCB. Experimentally, at higher excitation amplitudes, the parametric regime does dominate and the direct response no longer surfaces.

Despite the lower initiation threshold required to activate auto-parametric resonance, intentionally mismatching the natural frequencies as shown in Fig. 8a can offer additional frequency bandwidth for broader bandwidth operation. A partial overlap of the CCB frequency peak and the cantilever parametric peak can also achieve both broader operational frequency bandwidth and semi-resonant amplification of the base excitation to minimise initiation threshold.

Furthermore, for the data presented in Fig. 8, the half power bandwidth of the cantilever direct resonant peak is ~0.25 Hz while the cantilever parametric resonant peak is ~0.55 Hz. The general trend is an increasing half power bandwidth for the parametric resonant peak at higher acceleration levels due to deeper and more dominant operation into the instability region.

5. Conclusion and future work

This paper presents the potential of auto-parametric resonance for vibration energy harvesting. The parametric resonant phenomenon, when suitably engineered, is seen to outperform direct resonance in terms of power output. However, the excitation amplitude must attain a certain threshold prior to the onset of this alternative and superior resonant regime. The use of an initial spring to amplify the base excitation fed into the parametric resonator has shown nearly an order of magnitude lower initiation threshold amplitude (4.0 ms^{-2}) compared to a plain parametric resonator (>20 ms^{-2}). Furthermore, the incorporation of the auto-parametric phenomenon allows for resonant amplification of the base excitation and has demonstrated a further order of magnitude reduction in the initiation threshold amplitude (0.6 ms^{-2}).

This notable minimisation of the threshold enables the practical realisation of the mechanical amplification advantage of parametric resonance over direct resonance at low acceleration levels. Future work will address the optimisation of the piezoelectric transducer, such as the way it is attached to the substrate, to minimise loss

and enhance the absolute power level attainable. Incorporation of multi-degrees-of-freedom direct, parametric and auto-parametric resonators can serve to realise both frequency bandwidth and power level enhancements while reducing initiation thresholds.

Acknowledgement

This work was supported by the Engineering and Physical Sciences Research Council [grant number EP/I019308/1].

References

[1] S. Priya, D. Inman, Energy Harvesting Technologies, Springer US, New York, 2009.
[2] S. Beeby, N. White, Energy Harvesting for Autonomous Systems, Artech House, USA, 2010.
[3] G. Ye, J. Yan, Z. Wong, K. Soga, A. Seshia, Optimisation of a piezoelectric system for energy harvesting from traffic vibrations, in: IEEE International Ultrasonics Symposium Proceedings, Roma, Italy, 20–23 September, 2009, pp. 759–762.
[4] Z. Wong, J. Yan, K. Soga, A. Seshia, A multi-degree-of-freedom electrostatic mems power harvester, in: PowerMEMS, Washington, 1–4 December, 2009, pp. 300–303.
[5] G. Sebald, H. Kuwano, D. Guyomar, B. Ducharne, Experimental duffing oscillator for broadband piezoelectric energy harvesting, Smart Mater. Struct. 20 (10) (2011) 10.
[6] A. Erturk, D. Inman, Piezoelectric energy harvesting, Wiley, New Delhi, India, 2011.
[7] A. Arrieta, P. Hagedorn, A. Erturk, D. Inman, A piezoelectric bistable plate for nonlinear broadband energy harvesting, Appl. Phys. Lett. 97 (10) (2010), pp. 104 102–104 102–103.
[8] D. Zhu, S. Beeby, A coupled bistable structure for broadband vibration energy harvesting, in: Transducers, Barcelona, Spain, 2013, pp. 446–449, June.
[9] C. Trigona, F. Maiorca, B. Ando, S. Baglio, Tri-stable behaviour in mechanical oscillators to improve the performance of vibration energy harvesters, in: Transducers, Barcelona, Spain, 2013, pp. 458–461, June.
[10] C. McInnes, D. Gorman, M. Cartmell, Enhanced vibrational energy harvesting using nonlinear stochastic resonance, J. Sound Vib. 318 (4–5) (2008) 655–662.
[11] V. Challa, M. Prasad, F. Fisher, A coupled piezoelectric nelectromagnetic energy harvesting technique for achieving increased power output through damping matching, Smart Mater. Struct. 18 (9) (2009), 095029(11pp).
[12] J. Rastegar, C. Pereira, H.-L. Nguyen, Piezoelectric-based power sources for harvesting energy from platforms with low-frequency vibration, Proc. SPIE 6171 (2006), 617101-1-7.
[13] D. Lee, G. Carman, D. Murphy, C. Schulenburg, Novel micro vibration energy harvesting device using frequency up conversion, in: Transducers, Lyon, France, 2008, pp. 871–874, 10–14 June 2007.
[14] S. Priya, Modelling of electric energy harvesting using piezoelectric windmill, Appl. Phys. Lett. 87 (18) (2005) 3.
[15] J. Rastegar, R. Murray, Novel two-stage piezoelectric-based electrical energy generators for low and variable speed rotary machinery, SPIE Proc. 7288 (2009), pp. 72 880B–1–8.
[16] Y. Jia, J. Yan, K. Soga, A. Seshia, A parametrically excited vibration energy harvester, J. Intel. Mat. Syst. Str. 25 (3) (2013) 278–289.
[17] Y. Jia, A. Seshia, Directly and parametrically excited bi-stable vibration energy harvester for broadband operation, in: Proc. Transducers 2013, Barcelona, Spain, 16–20 June, 2013, pp. 454–457.
[18] Y. Jia, J. Yan, K. Soga, A.A. Seshia, Parametrically excited mems vibration energy harvesters with design approaches to overcome initiation threshold amplitude, J. Micromech. Microeng. 23 (11) (2013) 10.
[19] , in: Multi-frequency operation of a mems vibration energy harvester by accessing five orders of parametric resonance, J. Phys. Conf. Ser. (PowerMEMS 2013) 476 (1) (2013), London, 3–6 December 2013, pp. 607–611.
[20] M. Daqaq, C. Stabler, Y. Qaroush, T. Seuaciuc-Osorio, in: Investigation of power harvesting via parametric excitations, J. Intel. Mat. Syst. Str. 20 (5) (2009) 545–557.
[21] M. Daqaq, D. Bode, in: Exploring the parametric amplification phenomenon for energy harvesting, Proc. Inst. Mech. Eng. I J. Syst. Control Eng. 225 (4) (2011) 456–466.
[22] A. Nayfeh, D. Mook, Nonlinear Oscillations, Wiley-Interscience, New York, 1979.
[23] W. Thomson, in: M. Dahleh (Ed.), Theory of Vibration with Applications, 5th ed., Prentice-Hall, Inc., New Jersey, 1998.
[24] M. Cartmell, Introduction to Linear, Parametric and Nonlinear Vibrations, Chapman and Hall, London, 1990.
[25] N. Minorsky, Nonlinear Oscillations, Robert E. Krieger, New York, 1974.

Biographies

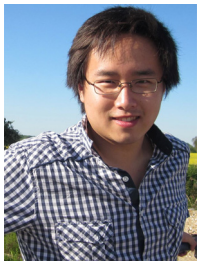

Yu Jia received a First Class (Honours) in MEng Electromechanical Engineering at the School of Electronics and Computer Science from the University of Southampton in 2010 and was award PhD in Engineering from the University of Cambridge in 2014. He is currently a Research Associate affiliated with the Cambridge University Nanoscience Centre and the Centre for Smart Infrastructure and Construction, with research interests involving vibration energy harvesting, MEMS, nonlinear vibration dynamics and smart systems.

Ashwin A. Seshia received his BTech in Engineering Physics in 1996 from IIT Bombay, MS and PhD degrees in Electrical Engineering and Computer Sciences from the University of California, Berkeley in 1999 and 2002 respectively. He joined the faculty of the Engineering Department at the University of Cambridge in October 2002 where he is presently a Reader in Microsystems Technology and a Fellow of Queens' College. His research interests include micro-fabricated devices and integrated microsystems, vibratory and resonant phenomena at the MEMS-scale, acoustic wave devices, resonators and oscillators, time and frequency metrology, transducers and interfaces, physical measurements at small length scales, sensors and sensor systems, vibration energy harvesting.